Materials Science & Engineering A 707 (2017) 419–425

Contents lists available at ScienceDirect

Materials Science & Engineering A

journal homepage: www.elsevier.com/locate/msea

Bimodal laminated Ti_3Al matrix composite achieved by *in situ* formed Ti_5Si_3 reinforcements

Tongtong Zhang[a], Guohua Fan[a,*], Kesong Miao[a], Kai Chen[b,*], Zhihao Pan[b], Shuai Chen[a], Xiping Cui[a], Meng Huang[a], Lin Geng[a]

[a] School of Materials Science and Engineering, Harbin Institute of Technology, Harbin 150001, China
[b] Center for Advancing Materials Performance from the Nanoscale (CAMP-Nano), State Key Laboratory for Mechanical Behavior of Materials, Xi'an Jiaotong University, Xi'an, Shaanxi 710049, China

ARTICLE INFO

Keywords:
Intermetallics
Microstructure
Phase transformation
Mechanical properties

ABSTRACT

The low density and high-temperature mechanical properties of intermetallic Ti_3Al based alloys are highly desirable for a wide range of critical applications. In this paper, we designed and prepared a novel laminated Ti_5Si_3/Ti_3Al composite (LTTC) consisting of alternating Ti_5Si_3-lean/coarse-grained Ti_3Al layers (TCLs) and Ti_5Si_3-rich/fine-grained Ti_3Al layers (TFLs). The processing route involves hot pressing of a stack of alternating Ti foils and Al-6Si foils, followed by a two-step reaction annealing. The tensile properties of the LTTC have also been evaluated, and the LTTC exhibited a good strength-ductility combination when compared with monolithic Ti_3Al. By in-depth mechanism discussion, we propose the possible approaches to further enhance the mechanical properties of such LTTC.

1. Introduction

Intermetallic Ti_3Al based alloys offer low density, high melting point, high thermal stability, and high creep resistance, and are thus attractive for many important high-temperature applications in aerospace, aircrafts and automobiles [1–4]. To enhance their high-temperature strengths [2,5,6], harder and stiffer ceramic particle reinforcements are introduced into the intermetallic Ti_3Al matrix to form composite materials. Tremendous efforts have been undertaken along this direction, and success have been reported in a wide range of reinforcement materials, such as carbides [7,8], borides [9,10], silicides [11–14], and so on. However, the composites suffer a major drawback: their limited ductility [15]. Therefore, it is hard to fabricate Ti_3Al composite sheets using traditional methods due to their poor hot workability. Researchers have fabricated a series of Ti-Al intermetallic sheets in a near-net shaping way by reaction synthesis of stacked dissimilar metal foils (Ti foils, Al foils or their composite foils, *etc.)* [7,10,16], which provides a suitable approach for large-scale industrial production of Ti-Al intermetallic sheets at low cost.

In recent years, in many classes of structural materials, to evade or alleviate the strength-ductility trade-off dilemma, the strategy of architecting microstructural heterogeneity has proven to be effective [17–21]. One effective way is by tailoring the grain size distribution. For instance, Wang et al. achieved a bimodal grain size distribution in pure Cu by applying a thermomechanical treatment, with micron-sized grains embedded in the nanocrystalline matrix [22]. Cu with such microstructure exhibited high strength, high tensile elongation, and high uniform elongation. Similarly, by embedding soft micrograined lamellae into hard ultrafine-grained lamella matrix, high tensile strength and high ductility were obtained simultaneously in pure Ti [23].

Besides, controlling the distribution of the reinforcements is also reported to be a strategy to obtain excellent mechanical properties [21]. It was demonstrated that 800 MPa high yield strength and amazing 40% tensile elongation could be achieved in Mo alloys at room temperature, by deploying the La_2O_3 nanoparticles uniformly in the interior of the micron sized crystal grain [24]. TiC was discovered to enhance the tensile strength of AlSi10 Mg. When its distribution was not delicately tailored, the elongation reduces, while once TiC particles distributed continuously at the AlSi10 Mg grain boundaries for form a ring structure, the elongation will not be traded off [25]. Combining these two strategies, it is appealing to develop an approach by which the reinforcement content and deployment can be controllable and simultaneously the grain size of the matrix can be tuned to obey the bimodal distribution.

In this article, we demonstrate a novel but simple method to manufacture heterogeneous LTTC. Our processing route involves three steps: hot pressing the stack of alternating Ti/Al-6Si foils, annealing at relatively low temperature, and finally annealing at high temperature.

* Corresponding authors.
E-mail addresses: ghfan@hit.edu.cn (G. Fan), kchenlbl@gmail.com (K. Chen).

http://dx.doi.org/10.1016/j.msea.2017.09.074
Received 24 June 2017; Received in revised form 15 September 2017; Accepted 16 September 2017
Available online 20 September 2017
0921-5093/

The final product consists of alternating TCLs and TFLs, which follows the bimodal microstructural design strategy introduced in the previous paragraph. From the mechanism discussion based on the microstructural characterization, we propose that the *in situ* formation of the Ti_5Si_3 reinforcement particles has the predominant impacts on the final microstructure of the LTTC products. Higher local Si concentration will produce higher number concentration of Ti_5Si_3 particles, which will constrain the coarsening of the Ti_3Al matrix grains, and thus result in the TFLs. Therefore, by controlling the thickness of stacking foils and the content of Si, the number concentration of the reinforcement, the thickness of the TCLs and TFLs, and the periodicity of the LTTC can all be tuned. With such an approach that can be readily adapted to industry, high performance LTTC materials can be designed and manufactured.

2. Materials and methods

2.1. Sample preparation

Commercial purity Ti foils (100 μm thick) and in-house fabricated Al-6Si alloy foils (30 μm thick) were cut into 100 mm × 100 mm squares. The chemical compositions of the raw materials are shown in Table 1. The Ti foils and Al-6Si foils were treated by 10 vol% HF and 10 vol% NaOH, respectively, to remove contaminants and oxide layers from the surfaces, and cleaned in an ultrasonic bath with acetone, and dried. Alternating commercial purity Ti foils (18 layers) and Al-6Si alloy foils (17 layers) were stacked, and followed by hot pressing under 40 MPa at 500 °C for 1 h to prepare laminated Ti-(Al-6Si) composite. Two annealing reactions were required to obtain the final LTTC product consisting of alternating TCLs and TFLs. The laminated Ti-(Al-6Si) composite was firstly annealed at low temperature (typically at 700 °C for 1 h) to complete the Ti-Al interdiffusion and form laminated Ti(Al,Si)-Ti$(Al,Si)_3$ composites. A second annealing was carried out at higher temperature (1250 °C for 1 h) under the pressure of 20 MPa to produce a fully dense LTTC. All of the three steps were carried out in vacuum ($\sim 10^{-2}$ Pa) within a high-strength graphite mold. The thickness of as-fabricated composites ranges from 2.0 mm to 2.2 mm.

2.2. Characterization

The microstructure of the fabricated composites was characterized using a scanning electron microscope (SEM, HELIOS NanoLab 600i) equipped with an energy dispersive X-ray spectrometer (EDS) and electron backscatter diffraction (EBSD). The phases in the composite were identified by X-ray diffraction (XRD, Philips X'Pert diffractometer). The matrix-reinforcement interface was observed in a transmission electron microscope (TEM, Tecnai G^2F30). The specimen for TEM observations was mechanically ground to a thickness of 50 μm, followed by punching to semi-disc with a diameter of 3 mm, and then ion-beam-milled using a Gatan Precision Ion Polishing System (PIPS, Gatan model 695). The density of the sample was determined by the Archimedes method, and the detailed description can be referred to Ref. [26].

Uniaxial tensile tests were conducted on an Instron-1186 testing machine at room temperature and elevated temperatures (600 °C and 700 °C) under a constant strain rate of $1 \times 10^{-4}\,s^{-1}$. At least three identical samples were measured at each temperature to ensure the reproducibility and reliability of the results. The plate-like tensile specimens with cross-section area of 2.5 mm × 2 mm and gauge length of 15 mm were machined with electrical discharges and their surfaces were carefully polished.

3. Results and discussion

3.1. Microstructure evolution of laminated Ti-(Al-6Si) composite

Fig. 1a shows the SEM micrograph under the back scattered electron (BSE) imaging mode of laminated Ti-(Al-6Si) composite after hot pressing at 500 °C for 1 h under 40 MPa. It is obvious that Ti and Al-6Si layers are parallel to each other with a good bonding. According to binary Al-Si phase diagram, the maximum solid solubility of Si in Al is only 1.5 at% at the eutectic temperature of 577 °C, and the value reduces to less than 0.05 at% at room temperature [27,28]. Due to the low solid solubility of Si in Al at room temperature, a large proportion of Si in Al-6Si alloy exists in the form of Si particles. As illustrated in Fig. 1b, the EDS result reveals that there is a thin diffusion layer with thickness of approximately 7 μm between Ti and Al-6Si layers. The XRD pattern in Fig. 2 indicates that only Al, Si, and Ti phases exist in the laminated Ti-(Al-6Si) composite, further demonstrating that no detectable reaction occurs after hot pressing.

Layered structure is obtained after the low temperature annealing at 700 °C for 1 h, as shown in Fig. 3. Periodic dark-bright strips are visualized in the SEM/BSE image (Fig. 3**a**). Almost all the dark layers are ~50 μm thick, about 30 μm thinner than the bright layers. From quantitative element analysis (Figs. 3**b**-3**e**), the ratio of Ti and (Al + Si) in the dark layers is approximately 1:3, in good agreement with the previously reported $Ti(Al,Si)_3$, which has the same structure as $TiAl_3$ except that some of the Al atoms are replaced by Si atoms [29]. The bright layers are composed of Ti(Al,Si) alloy, formed due to the diffusion of Al and Si from Al-6Si alloy foils to Ti foils. As shown in Fig. 3b and e, it is clear that the Si concentration in the laminated Ti(Al,Si)-Ti$(Al,Si)_3$ composites is characterized by layer distribution, namely Ti$(Al,Si)_3$ layers with high Si concentration (~7.6 at%) while residual Ti layers with relatively low Si concentration (~1.2 at%). In addition, the maximum value of Si concentration (~9.0 at%) appears at the center of the $Ti(Al,Si)_3$ layer, and then decreases away from the center. This indicates that there is a composition gradient of Si in the $Ti(Al,Si)_3$ layer and the distribution of Si is controlled by diffusion. That is to say, the distribution of Si can be tailored easily by adjusting low temperature annealing parameters. In the SEM/BSE images, micrometer sized voids are observed concentrated and aligned at the middle along the thickness direction of the dark $Ti(Al,Si)_3$ layers.

As shown in Fig. 4, the XRD pattern shows that the diffraction peaks of Si disappeared, and only Ti and $TiAl_3$ phases existed after low temperature annealing, further proving that Al converts into $TiAl_3$ completely. The solid solubility of Si in $TiAl_3$ could reach 15 at% at room temperature [30,31], and thus Si mainly dissolves into the $TiAl_3$ to form $Ti(Al,Si)_3$ due to the high solid solubility of Si in $TiAl_3$, which is consistent with the SEM results in Fig. 3.

3.2. Microstructure characterization of laminated Ti_5Si_3/Ti_3Al composite

The microstructure of LTTC after the high temperature annealing at 1250 °C for 1 h is demonstrated in Fig. 5. Alternating TCLs (about 80 μm thick) and TFLs (approximately 40 μm thick) are distinguished in the SEM image under secondary electron (SE) mode in Fig. 5**a**. An area

Table 1
Chemical compositions of the raw materials (wt%).

Materials	Si	Fe	Cu	N	C	O	H	Mn	Mg	Zn	Ti	Al
Ti	0.01	0.25	–	0.03	0.10	0.20	0.02	–	–	–	Bal.	–
Al − 6Si	6.0	0.80	0.30	–	–	–	–	0.05	0.05	0.10	0.20	Bal.

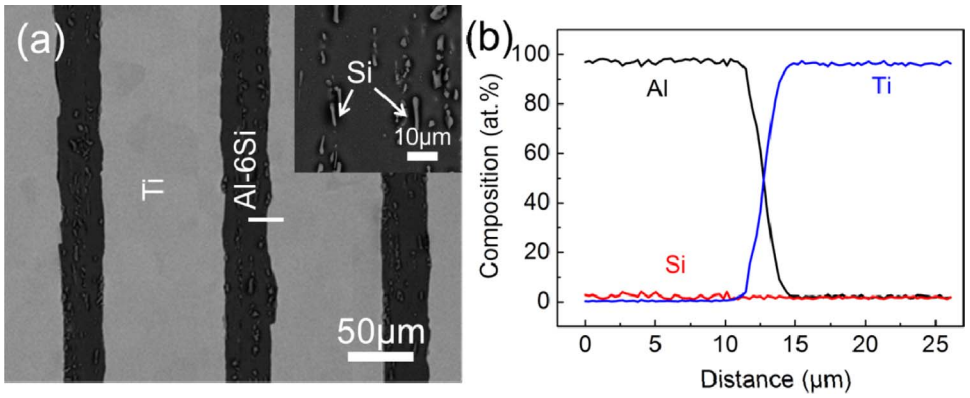

Fig. 1. Microstructure and composition profiles of laminated Ti-(Al-6Si) composite after hot pressing at 500 °C for 1 h under 40 MPa: (a) SEM image; (b) Composition profiles from left to right along the white line in (a).

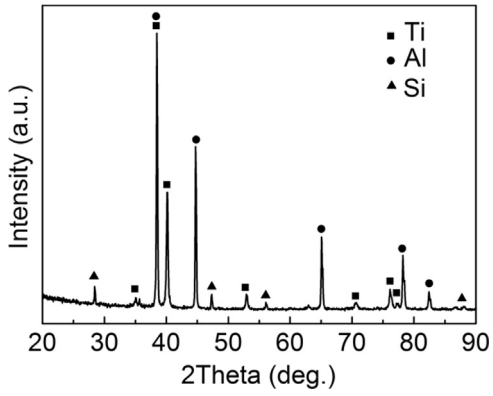

Fig. 2. XRD pattern of laminated Ti-(Al-6Si) composite.

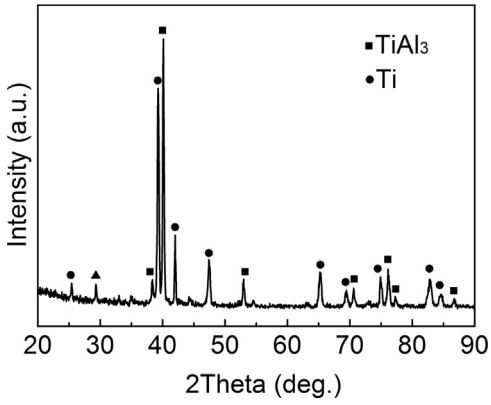

Fig. 4. XRD pattern of laminated Ti-(Al-6Si) composite after initial annealing at 700 °C for 1 h.

including the TCL-TFL interface is enlarged in Fig. 5**b**. The one dimensional EDS characterization (Fig. 5**c**) proves that the chemical composition is identical across the interface, suggesting that the SEM/SE contrast in fact results from the different number density of the Ti_5Si_3 reinforcements, in lieu of the matrix. The XRD result shown in Fig. 5**d** further confirms that the resulting LTTC only contains the Ti_5Si_3 reinforcements and Ti_3Al matrix, and no other phases exist.

As shown in Fig. 6, EBSD analysis of the selected region indicates that both the TCL and TFL consist of Ti_3Al structure. The average grain size of the Ti_3Al crystals in the TCLs and TFLs is measured to be approximately 55 μm and 12 μm, respectively. The Ti_5Si_3 reinforcement particles, which appear brighter in the SEM/SE image, have an average diameter of about 0.3 μm in both TCLs and TFLs. In the TFLs, the volume fraction of Ti_5Si_3 particles is larger than 10%, whereas it is only about 2.3% in the TCLs. From the inverse pole figures along the normal direction (ND) display two preferred orientations in the TFLs, one close to $[11\bar{2}0]$ and the other close to $[10\bar{1}2]$, while in the TCLs, the crystal

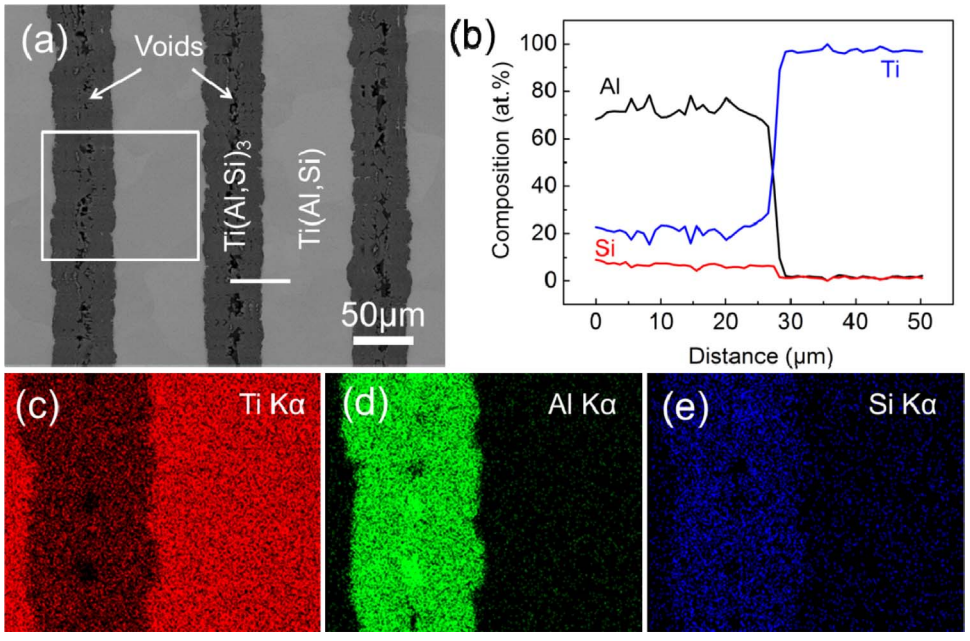

Fig. 3. Microstructure and composition profiles of laminated Ti-(Al-6Si) composite after initial annealing at 700 °C for 1 h: (a) SEM image; (b) Composition profiles from left to right along the white line in (a); (c-e) Element distribution of Ti, Al, and Si in the rectangular region marked in (a).

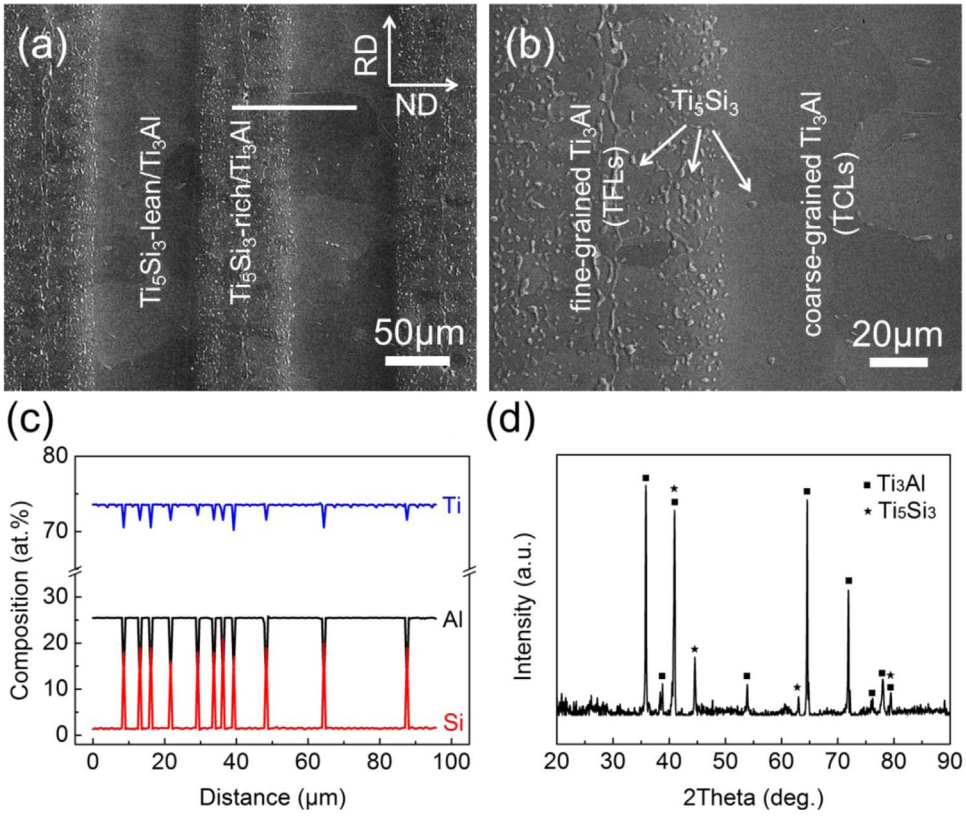

Fig. 5. Microstructure of the resulting LTTC: (a) low- and (b) high-magnification SEM maps showing the layered architecture consisting of alternating Ti_5Si_3-lean/coarse-grained Ti_3Al layers and Ti_5Si_3-rich/fine-grained Ti_3Al layers; (c) Composition profiles from left to right along the white line in (a); (d) XRD pattern. The spatial coordinate system is represented by rolling (RD), normal (ND), and transverse (TD) direction.

orientation distribution is transversely isotropic (Fig. 6**b**). Moreover, these two IPFs are with different color scale, indicating that the grains in the TFLs possess stronger preferred orientation than the ones in the TCLs.

The interface between the matrix and the reinforcement plays a key part in the development of high-performance composites [32]. The microstructure of the LTTC is further revealed by TEM and high-resolution TEM (HRTEM) in Fig. 7. The TEM bright field image demonstrates that the interface between *in situ* Ti_5Si_3 particle and Ti_3Al matrix is clear, as shown in Fig. 7**a**. The HRTEM image of a representative interfacial region between Ti_5Si_3 particle and Ti_3Al matrix is shown in Fig. 7**b**. Its fast Fourier transformation (FFT) pattern presented in Fig. 7**b** indicates no obvious orientation relationship between the matrix and reinforcement phases. From both XRD and TEM results, no other precipitations and residual reactants are detected in the LTTC, which indicates better binding force between *in situ* Ti_5Si_3 particle and Ti_3Al matrix.

3.3. Formation mechanism of laminated Ti_5Si_3/Ti_3Al composite

We first discuss the formation mechanism of the LTTC as a direct consequence of *in situ* formed Ti_5Si_3 reinforcements in detail. The laminated Ti(Al,Si)-Ti(Al,Si)$_3$ structure obtained after the first annealing results from the interdiffusion and reaction between Al-Si and Ti. After Ti foils and Al-6Si foils are hot pressed together, at 700 °C, Al-6Si melts but Ti stays at solid state, and thus they diffuse into each other to form Al(Ti,Si) liquid solution and Ti(Al,Si) solid solution. It appears that $TiAl_3$ phase nucleates predominantly from the liquid Al(Ti,Si) solution and Ti(Al,Si) solid solution, and then Al is completely consumed and $TiAl_3$ is the only product at this stage [30,33]. Considering that the theoretical maximum concentration of Si in the $TiAl_3$ is 15 at% at room temperature [30], therefore a fraction of Si dissolves in the $TiAl_3$ to form Ti(Al,Si)$_3$ rather than to form silicon or silicide precipitates. It is important to emphasize that during the holding time, the Si concentration is of a certain composition gradient in Ti(Al,Si)$_3$, which is controlled by diffusion process. Meanwhile, Si atoms keep diffusing into

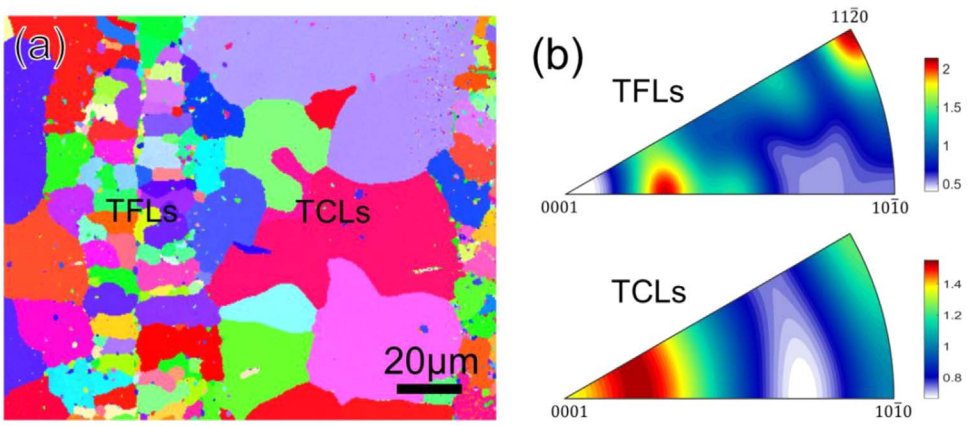

Fig. 6. Microstructure of the LTTC: (a) Inverse pole figure (IPF) maps; (b) ND-IPFs of the TFLs and TCLs, respectively.

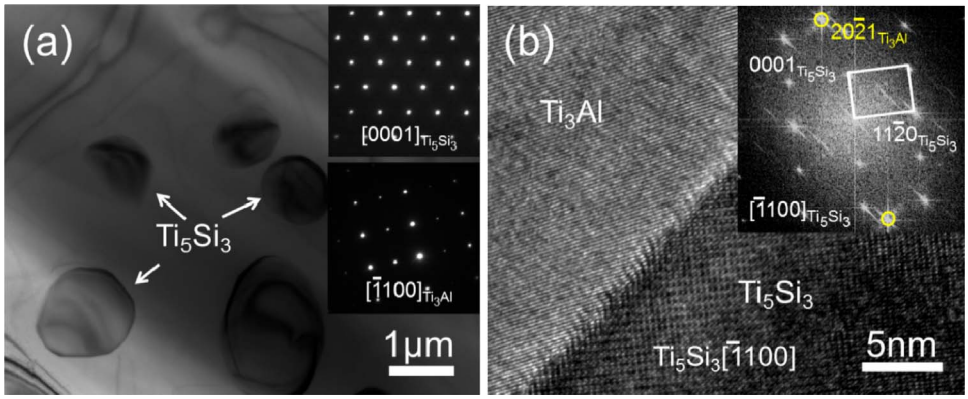

Fig. 7. The TEM microstructure of the LTTC: (a) bright field image of *in situ* Ti_5Si_3; (b) HRTEM image of interface between α_2-Ti_3Al matrix and *in situ* Ti_5Si_3 and corresponding FFT pattern.

remaining solid Ti due to concentration gradient. From Fick's second law, extending the holding time and temperature will enhance the Si concentration in Ti(Al,Si) while lower that in $Ti(Al,Si)_3$. Therefore, we propose that by tuning the starting foil materials and annealing parameters, the distributed concentration of Si is controllable, which, as will be explain later, is the key to obtain the bimodal matrix grain distribution.

Due to the unmatched diffusivity between Ti and Al during the first annealing, Kirkendall voids formed in the $Ti(Al,Si)_3$ layers. As stress concentrators, the voids may enhance non-uniform deformation, induce crack formation, and eventually cause disastrous failures. As a result, in the subsequent second annealing, the pressure of 20 MPa is employed to eliminate these voids successfully.

After the low temperature annealing, the average concentration of Si in the Ti(Al,Si) layers is low (only 1.2 at%) as shown in Fig. 3. During the subsequent high temperature annealing at 1250 °C, the solid-state reaction is dominated by the diffusion process due to the presence of concentration gradient in the laminated Ti(Al,Si)-$Ti(Al,Si)_3$ composite. It is well known that several other Ti-Al intermetallic compounds, including TiAl, $TiAl_2$, and Ti_3Al could be formed between Ti and $TiAl_3$ [7,10]. The maximum solid solubility of Si in TiAl, and $TiAl_2$ are 0.8 at % and 1.5 at%, respectively, which are much lower than that in α-Ti and $TiAl_3$ (2.3 at% and 15 at%, respectively) [30,33]. Accompanying with the formation of TiAl and $TiAl_2$, because of low solid solubility of Si in TiAl and $TiAl_2$, a number of Si in the Ti(Al,Si) layers precipitates in the predominant form of Ti_5Si_3 particles in the TiAl and $TiAl_2$ layers. The low concentration of Si in the Ti(Al,Si) layers results in a low number density of Ti_5Si_3 particles. The Ti_3Al matrix would continue to be produced *via* a series of solid-solid transformations with further diffusion. It should be noted that the grains would grow and coarsen during the annealing for long time [34,35]. However, it has been reported that the presence of *in situ* formed particles could constrain the grain migration, growth, and coarsening, and thereby refine the matrix grains [24,34,36,37]. The restricting effect imposed by a low number density of *in situ* Ti_5Si_3 particles hinders the Ti_3Al grain boundaries migration to some extent, therefore the TCLs are formed in the original Ti(Al,Si) layers and the eventual grain size of Ti_3Al matrix in the TCLs is slightly large (approximately 55 μm) as shown in Fig. 6. We note that the average concentration of Si in the $Ti(Al,Si)_3$ layers derived from the low temperature annealing is much higher (7.6 at%) than that in the Ti (Al,Si) layers as shown in Fig. 3. As we discuss above, large amounts of *in situ* Ti_5Si_3 particles would precipitate in the original $Ti(Al,Si)_3$ layers during high temperature annealing. Therefore, higher number density of reinforcement particles interact with the migrating grain boundaries and restrict the growth and coarsening of Ti_3Al grains more effectively, and the Ti_3Al grains get to stay at small sizes of only 15 μm as shown in Fig. 6. This is the reason that the Ti_3Al grains in the TFLs have an average size smaller than that in the TCLs. The high temperature annealing time was extended to 1 h to ensure all reactions are sufficient for the formation of equilibrium Ti_3Al in this system, and thus eventually the LTTC consisting of alternating TCLs and TFLs is achieved. The crystal orientations in the TFLs and TCLs may have inherited the texture of $Ti(Al,Si)_3$ and Ti(Al,Si), respectively, but this postulate needs to be further confirmed with more systematic investigations. In summary, in both the $Ti(Al,Si)_3$ layers and Ti(Al,Si) layers, Ti_5Si_3 particles *in situ* formed, and the density of the reinforcements predominantly depend on the concentration of Si.

As discussed above, a considerable fraction of Ti_5Si_3 reinforcements *in situ* precipitate during the second annealing when $Ti(Al,Si)_3$ and Ti (Al,Si) transforms to $TiAl_2$, and TiAl, which is before the formation of the Ti_3Al matrix. These *in situ* formed particles constrain the grain migration, growth, and coarsening of the matrix grains, and thus the matrix grain size is reversely proportional to the number density of the reinforcement particles. In other words, if the reinforcement particles did not *in situ* form before the matrix grains, they could probably not influence the matrix grain and achieve bimodal distribution. In our work, by using the commercial purity Ti foils and Al-6Si foils as the starting materials, the concentration distribution of Si is readily controlled, and by nature the silicide reinforcement particles *in situ* grow before the appearance of the final matrix grains. Therefore, the bimodal matrix grain size distribution is readily obtained using our method.

3.4. Tensile properties

The tensile properties at different temperatures (25 °C, 600 °C, and 700 °C, respectively) obtained from uniaxial tensile tests for LTTC are presented in Fig. 8. The ultimate tensile strengths (σ_{UTS}) at 25 °C, 600 °C, and 700 °C were 255 MPa, 463 MPa and 451 MPa, respectively. Generally, the total elongation at fracture (ε_f) of monolithic Ti_3Al was less than 3% when the tensile temperature was below 700 °C [38]. However, the LTTCs exhibit a highest tensile strength of 463 MPa with a total elongation at fracture of 3.4% at 600 °C, comparable to as-cast Ti-24Al-11 Nb-5Si alloys [39]. In particular, with the temperature rising from 600 °C to 700 °C, the total elongation at fracture of the LTTC showed a remarkable increase, indicating that the ductility-brittleness

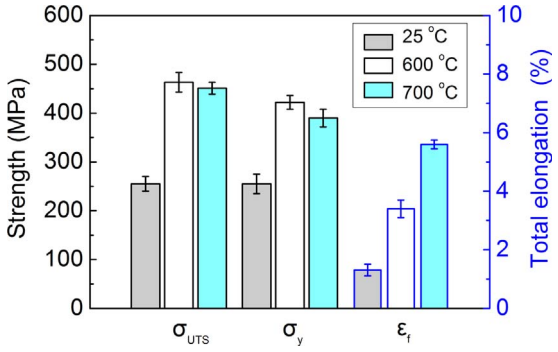

Fig. 8. Tensile properties of the LTTC measured at different temperatures.

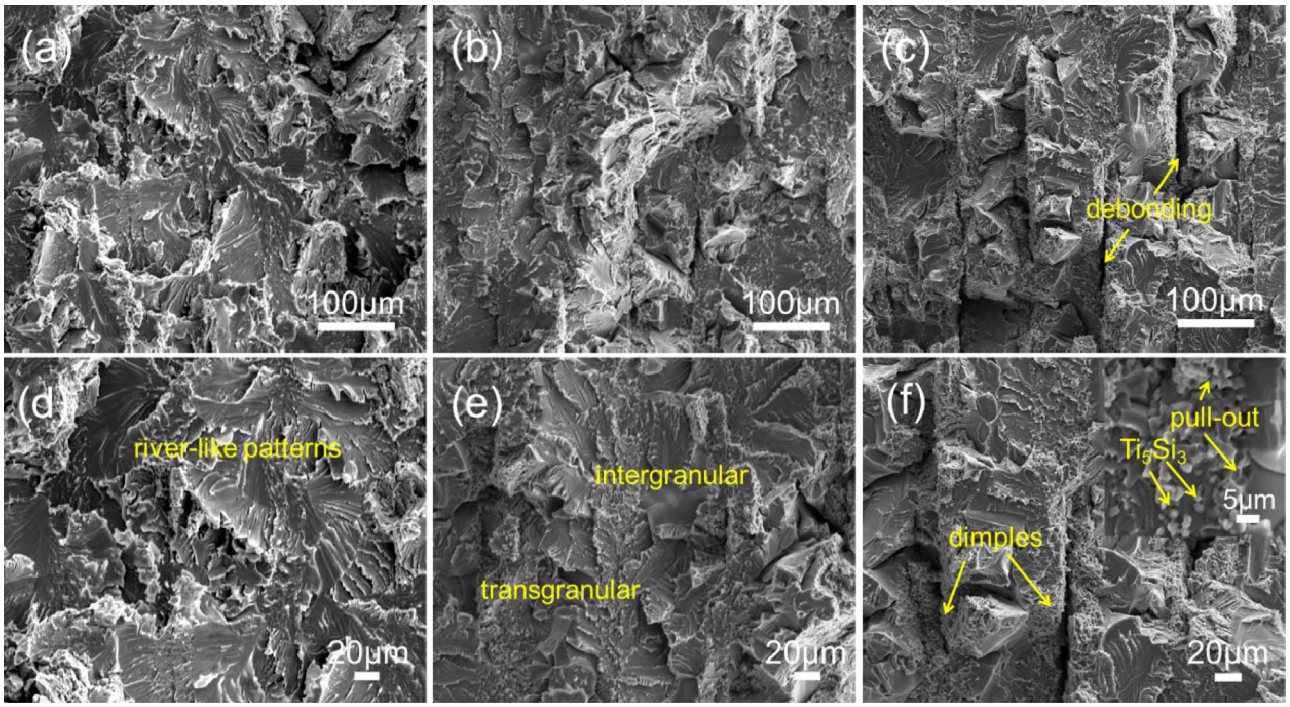

Fig. 9. The fracture surfaces of the LTTC tested at different temperatures: (a) 25 °C, (b) 600 °C and (c) 700 °C; (d), (e) and (f) are high-magnification micrographs corresponding to (a), (b) and (c), respectively.

transition temperature (DBTT) of the LTTC was below 700 °C. Meanwhile, it is worth noting that the density of the composites is only 4.21 g/cm^3, which is over 17% lower than that of the Ti_2AlNb alloys (5.1 g/cm^3 or higher).

The fracture surfaces of the LTTC tested at room temperature, 600 °C and 700 °C were shown in Fig. 9, respectively. The overall fracture surfaces of the specimens tested at room temperature were relatively flat. The obvious river-like patterns were observed, indicating typical brittle cleavage fracture mode in the fracture surface (Fig. 9a and d). By contrast, with increasing temperature to 600 °C, the fracture morphologies of the LTTC change from flat to tortuous features as shown in Fig. 9b and e. It is obvious that the transgranular fracture still is the main fracture mechanism for the TCLs, while in addition to transgranular fracture, intergranular fracture appeared in the TFLs because of the fine grains. At the temperature above the BDTT (700 °C), signs of ductile fracture can be identified in the LTTC. Observations of fracture surfaces show different fracture modes in the TCLs and TFLs (Fig. 9b and e), which is intimately correlated with their grain size. In comparison with the fracture surfaces at 600 °C, the intergranular failure significantly increased in the TCLs, as shown in Fig. 9f. Meanwhile, the fracture morphology of TFLs reveals the ductile fracture characteristic with many fine dimples. In addition, the pull-out of a number of Ti_5Si_3 particles from the Ti_3Al matrix and local interface delamination were observed in Fig. 9c and f. This implied that *in situ* Ti_5Si_3 particles could withstand the load from the Ti_3Al matrix, resulting in an enhancement of tensile strength. In general, the fracture manner of the LTTC transforms from brittle cleavage fracture at room temperature into ductile mode with increasing temperature.

It was believed that the bimodal grain structure and reinforcement distribution are two important factors that influence the performance of the LTTCs. We have to admit that the performance of the LTTCs can be further advanced by tailoring the bimodal grain structure and reinforcement distribution [21,23,24,40–42]. One possibility is to further refine the size of the reinforcements and the matrix grains to submicron or even nanometer regime to obtain dramatic tensile strength and ductility simultaneously, as reported elsewhere [43]. As we have shown in the preceding paragraphs, higher number density of reinforcement particles will help refine the matrix grain size. Therefore, by enhancing the mass fraction of Si in the Al-Si alloy and reducing the initial foil thickness, finer grains can be achieved. The development of such light-weighted LTTCs opens a new way for designing high performance IMCs.

4. Conclusions

In summary, a combination of the two strategies, namely bimodal grain structure and controlled reinforcement distribution, is proposed to optimize the strength and ductility of Ti_3Al matrix composites. To this end, commercially pure Ti foils and Al-Si foils are used to produce LTTC consisting of alternating TCLs and TFLs by hot pressing and two-step reaction annealing. Detailed microstructure characterization reveals that the fine grained Ti_3Al layers are obtained due to the *in situ* formation of high density reinforcement particles, while matrix grains are coarsened in absence of the constraint of Ti_5Si_3. In brief, the grain size and reinforcement number density obey a reverse proportional relationship. The mechanical behaviors of the LTTCs are advanced and comparable with the Ti_2AlNb alloys, but the density is significantly lower. We also discussed the possible approaches to further optimize the microstructure and promote the mechanical performance of the LTTCs. As a consequence, this work is amenable to large-scale industrial production and offers the essential guidance to the fabrication, investigation and application of Ti_3Al matrix composites.

Acknowledgements

This research was financially supported by the National Key research & development Plan (NO. 2017YFB0703100), the National Natural Science Foundation of China (grant numbers 51571070, 51571071, 51671154) and the National Basic Research Program of China (“973” Program) (grant number 2015CB057400). We also appreciate the support from the International Joint Laboratory for Micro/Nano Manufacturing and Measurement Technologies and the Collaborative Innovation Center of High-End Manufacturing Equipment.

References

[1] Y.W. Kim, Intermetallic alloys based on gamma titanium aluminide, JOM 41 (1989) 24–30.
[2] Y. Koizumi, T. Nakano, Y. Umakoshi, Plastic deformation and fracture behaviour of Ti_3Al single crystals deformed at high temperatures under cyclic loading, Acta Mater. 47 (1999) 2019–2029.
[3] X.P. Cui, G.H. Fan, L.J. Huang, J.X. Gong, H. Wu, T.T. Zhang, L. Geng, S.H. Meng, Preparation of a novel layer-structured Ti_3Al matrix composite sheet by liquid-solid reaction between Al foils and TiB/Ti composite foils, Mater. Des. 101 (2016) 181–187.
[4] H. Wu, G.H. Fan, B.C. Jin, L. Geng, X.P. Cui, M. Huang, X.C. Li, S. Nutt, Enhanced fracture toughness of TiBw/Ti_3Al composites with a layered reinforcement distribution, Mater. Sci. Eng. A 670 (2016) 233–239.
[5] R.J. Kerans, Deformation in Ti_3Al fatigued at room and elevated temperatures, Metall. Trans. A 15 (1984) 1721–1729.
[6] K.S. Chan, Understanding fracture toughness in gamma TiAl, JOM 44 (1992) 30–38.
[7] H. Wu, G.H. Fan, X.P. Cui, L. Geng, F. Yuan, J.C. Pang, L.S. Wei, M. Huang, Mechanical properties of ($Ti_2AlC+Ti_3AlC$)-TiAl ceramic-intermetallic laminate (CIL) composites, Mater. Sci. Eng. A 585 (2013) 439–443.
[8] S.L. Shu, F. Qiu, S.J. Lu, S.B. Jin, Q.C. Jiang, Phase transitions and compression properties of Ti_2AlC/TiAl composites fabricated by combustion synthesis reaction, Mater. Sci. Eng. A 539 (2012) 344–348.
[9] M.L. Vanmeter, S.L. Kampe, L. Christodoulou, Mechanical properties of near-γ titanium aluminides reinforced with high volume percentages of TiB_2, Scr. Mater. 34 (1996) 1251–1256.
[10] X.P. Cui, G.H. Fan, L. Geng, Y. Wang, H.W. Zhang, H.X. Peng, Fabrication of fully dense TiAl-based composite sheets with a novel microlaminated microstructure, Scr. Mater. 66 (2012) 276–279.
[11] K.P. Rao, J.B. Zhou, Characterization and mechanical properties of in situ synthesized Ti_5Si_3/TiAl composites, Mater. Sci. Eng. A 356 (2003) 208–218.
[12] T. Klassen, C. Suryanarayana, R. Bormann, Low-temperature superplasticity in ultrafine-grained Ti_5Si_3-TiAl composites, Scr. Mater. 59 (2008) 455–458.
[13] F.S. Sun, F.H.S. Froes, Precipitation of Ti_5Si_3 phase in TiAl alloys, Mater. Sci. Eng. A 328 (2002) 113–121.
[14] A.B. Li, X.P. Cui, G.S. Wang, W. Qu, F. Li, X.X. Zhang, W.C. Gan, L. Geng, S.H. Meng, Fabrication of in situ Ti_5Si_3/TiAl composites with controlled quasi-network architecture using reactive infiltration, Mater. Lett. 185 (2016) 351–354.
[15] S. Djanarthany, J.C. Viala, J. Bouix, An overview of monolithic titanium aluminides based on Ti_3Al and TiAl, Mater. Chem. Phys. 72 (2001) 301–319.
[16] L.M. Peng, J.H. Wang, H. Li, J.H. Zhao, L.H. He, Synthesis and microstructural characterization of Ti-Al_3Ti metal-intermetallic laminate (MIL) composites, Scr. Mater. 52 (2005) 243–248.
[17] A. Devaraj, V.V. Joshi, A. Srivastava, S. Manandhar, V. Moxson, V.A. Duz, C. Lavender, A low-cost hierarchical nanostructured beta-titanium alloy with high strength, Nat. Commun. 7 (2016) 11176.
[18] T.H. Fang, W.L. Li, N.R. Tao, K. Lu, Revealing extraordinary intrinsic tensile plasticity in gradient nano-grained copper, Science 331 (2011) 1587–1590.
[19] Y. Wei, Y. Li, L. Zhu, Y. Liu, X. Lei, G. Wang, Y. Wu, Z. Mi, J. Liu, H. Wang, H. Gao, Evading the strength-ductility trade-off dilemma in steel through gradient hierarchical nanotwins, Nat. Mater. 5 (2014) 3580.
[20] X.L. Wu, F.P. Yuan, M.X. Yang, P. Jiang, C.X. Zhang, L. Chen, Y.G. Wei, E. Ma, Nanodomained nickel unite nanocrystal strength with coarse-grain ductility, Sci. Rep. 5 (2015) 11728.
[21] L.J. Huang, L. Geng, H.X. Peng, Microstructurally inhomogeneous composites: is a homogeneous reinforcement distribution optimal? Prog. Mater. Sci. 71 (2015) 93–168.
[22] Y. Wang, M. Chen, F. Zhou, E. Ma, High tensile ductility in a nanostructured metal, Nature 419 (2002) 912–915.
[23] X.L. Wu, M.X. Yang, F.P. Yuan, G.L. Wu, Y.J. Wei, X.X. Huang, Y.T. Zhu, Heterogeneous lamella structure unites ultrafine-grain strength with coarse-grain ductility, Proc. Natl. Acad. Sci. USA 112 (2015) 14501–14505.
[24] G. Liu, G.J. Zhang, F. Jiang, X.D. Ding, Y.J. Sun, J. Sun, E. Ma, Nanostructured high-strength molybdenum alloys with unprecedented tensile ductility, Nat. Mater. 12 (2013) 344–350.
[25] D. Gu, H. Wang, D. Dai, P. Yuan, W. Meiners, R. Poprawe, Rapid fabrication of Al-based bulk-form nanocomposites with novel reinforcement and enhanced performance by selective laser melting, Scr. Mater. 96 (2015) 25–28.
[26] M.J. Keenan, M. Hegsted, K.L. Jones, J.P. Delany, J.C. Kime, L.E. Melancon, R.T. Tulley, K.D. Hong, Comparison of bone density measurement techniques: DXA and Archimedes' principle, J. Bone Miner. Res. 12 (1997) 1903–1907.
[27] J.L. Murray, A.J. Mcalister, The Al-Si (Aluminum-Silicon) system, J. Phase Equil. 5 (1984) 74–84.
[28] J.H. Li, M. Albu, F. Hofer, P. Schumacher, Solute adsorption and entrapment during eutectic Si growth in A-Si-based alloys, Acta Mater. 83 (2015) 187–202.
[29] Q.D. Qin, Y.G. Zhao, C. Liu, W. Zhou, Q.C. Jiang, Development of aluminium composites with in situ formed AlTiSi reinforcements through infiltration, Mater. Sci. Eng. A 460–461 (2007) 604–610.
[30] V. Raghavan, Al-Si-Ti (Aluminum-Silicon-Titanium), J. Phase Equilib. Diff. 30 (2009) 82–83.
[31] T.T. Zhang, G.H. Fan, H. Wu, X.P. Cui, M. Huang, K.S. Miao, L. Geng, Atomic-scale analysis of early-stage precipitation in Ti$(Al,Si)_3$ alloy, Mater. Des. 134 (2017) 244–249.
[32] S.J. Kang, Y.W. Kim, M. Kim, J.M. Zuo, Determination of interfacial atomic structure, misfits and energetics of Ω phase in Al-Cu-Mg-Ag alloy, Acta Mater. 81 (2014) 501–511.
[33] Z. Li, C.L. Liao, Y.X. Liu, X.M. Wang, Y. Wu, M.X. Zhao, Z.H. Long, F.C. Yin, 700 °C isothermal section of the Al-Ti-Si ternary phase diagram, J. Phase Equilib. Diff. 35 (2014) 564–574.
[34] C.L. Yang, B. Zhang, D.C. Zhao, H.B. Lü, T.G. Zhai, F. Liu, Microstructure and mechanical properties of AlN particles in situ reinforced Mg matrix composites, Mater. Sci. Eng. A 674 (2016) 158–163.
[35] Y. Xiong, T.T. He, H.P. Li, Y. Lan, F.Z. Ren, A.A. Volinsky, Annealing effects on microstructure and mechanical properties of cryorolled Fe-25Cr-20Ni steel, Mater. Sci. Eng. A 703 (2017) 68–75.
[36] A. Moradkhani, H. Baharvandi, M.M. Mohammadi Samani, Mechanical properties and microstructure of B_4C-NanoTiB_2-Fe/Ni composites under different sintering temperatures, Mater. Sci. Eng. A 665 (2016) 141–153.
[37] S.H. Kim, H. Kim, N.J. Kim, Brittle intermetallic compound makes ultrastrong low-density steel with large ductiity, Nature 518 (2015) 77–79.
[38] S. Djanarthany, J.C. Viala, J. Bouix, An overview of monolithic titanium aluminides based on Ti_3Al and TiAl, Mater. Chem. Phys. 72 (2001) 301–319.
[39] L.T. Zhang, J.S. Wu, W. Hua, G.H. Qiu, Strength and fracture of two hot-rolled Ti-Al-Si-Nb dual phase alloys based on Ti_3Al, Intermetallics 8 (2000) 709–716.
[40] D. Witkin, Z. Lee, R. Rodriguez, S. Nutt, E. Lavernia, Al-Mg alloy engineered with bimodal grain size for high strength and increased ductility, Scr. Mater. 49 (2003) 297–302.
[41] X. Zhang, H. Wang, R.O. Scattergood, J. Narayan, C.C. Koch, A.V. Sergueeva, Studies of deformation mechanisms in ultra-fine-grained and nanostructured Zn, Acta Mater. 50 (2002) 4823–4830.
[42] C. Koch, Optimization of strength and ductility in nanocrystalline and ultrafine grained metals, Scr. Mater. 49 (2003) 657–662.
[43] K. Lu, The future of metals, Science 328 (2010) 319–320.